



Spatial coefficient of variation of arterial spin labeling MRI for detecting hemodynamic disturbances measured with ^{15}O -gas PET in patients with moyamoya disease

Shoko Hara^{1,2} · Yoji Tanaka¹ · Motoki Inaji^{1,2} · Shihori Hayashi^{1,2} · Kenji Ishii² · Tadashi Narai^{1,2} · Taketoshi Maehara¹

Received: 2 June 2021 / Accepted: 30 August 2021 / Published online: 9 September 2021
© The Author(s), under exclusive licence to Springer-Verlag GmbH Germany, part of Springer Nature 2021

Abstract

Purpose The aim of this study was to investigate whether the spatial coefficient of variation of arterial spin labeling (ASL-CoV) acquired in clinical settings can be used to estimate the hemodynamic disturbances measured with ^{15}O -gas positron emission tomography (PET), especially an increased oxygen extraction fraction (OEF), in patients with moyamoya disease.

Methods We evaluated 68 adult patients with moyamoya disease who underwent ASL (postlabeling delay (PLD) = 1525 ms and 2525 ms) and PET. Regional values were measured using the middle cerebral artery territorial atlas divided into proximal, middle, and distal regions based on the arterial transit time, and correlations of ASL-CoV with cerebral blood flow, cerebral blood volume, mean transit time, and OEF, as well as the relationship between increased OEF and ASL-CoV, were evaluated.

Results Regardless of the choice of region and PLD, ASL-CoV was significantly correlated with PET-measured parameters, including OEF ($|r|=0.30\text{--}0.80$, $P<0.001$). Regions with an increased OEF showed a significantly higher ASL-CoV than regions with a nonincreased OEF ($P\leq 0.03$) regardless of the choice of region and PLD. The accuracy of identification of an increased OEF was highest when using a PLD of 1525 ms and the middle region (area under the curve = 0.750; using a cutoff value of 31.27, sensitivity = 97.4%, specificity = 41.7%, negative predictive value = 92.6%, and positive predictive value = 67.9%).

Conclusion ASL-CoV may help identify patients with increased OEF.

Keywords Arterial spin labeling · Spatial coefficient of variation · Cerebral hemodynamics · Moyamoya disease · Oxygen extraction fraction · Perfusion imaging

Introduction

Moyamoya disease (MMD) is a progressive steno-occlusive disease affecting the circle of Willis that ultimately leads to marked leptomeningeal anastomosis and basal moyamoya vessels [1]. Because of the diverse heterogeneity of

the collateral status among patients, perfusion studies are indispensable in determining the need for revascularization surgery [2]. The criterion standard of perfusion imaging is ^{15}O -gas positron emission tomography (PET), which can measure the oxygen extraction fraction (OEF), which is a biomarker of misery perfusion [3]. However, PET is costly, invasive, and not readily available in most institutes. One of the most noninvasive techniques for analyzing perfusion is arterial spin labeling magnetic resonance imaging (ASL-MRI), which uses endogenous water as the tracer [4]. Previous studies have reported good correlations between cerebral blood flow values measured with ASL (ASL-CBF) and CBF measured with PET (PET-CBF) in normal volunteers [5] and in patients with MMD [6, 7]. However, to date, the ability of quantitative ASL-CBF to predict misery perfusion, i.e., an increased OEF, has been unsatisfactory in patients with

✉ Shoko Hara
shara.nsrq@tmd.ac.jp

Yoji Tanaka
tanaka.nsrq@tmd.ac.jp

¹ Department of Neurosurgery, Tokyo Medical and Dental University, 1-5-45 Yushima, Bunkyo-ku, Tokyo 113-8519, Japan

² Research Team for Neuroimaging, Tokyo Metropolitan Institute of Gerontology, 35-2 Sakaecho, Itabashi-ku, Tokyo, Japan

MMD, especially when acquired using a single postlabeling delay (PLD).

Recently, the spatial coefficient of variation of ASL (ASL-CoV) calculated by dividing the standard deviation (SD) by the average regional value was proposed for detecting hemodynamic disturbances using a single PLD [8]. In previous studies, ASL-CoV correlated with the mean transit time (MTT) measured by PET and the arterial transit time (ATT) measured by pulsed ASL in patients with carotid artery stenosis [9], as well as time-based parameters measured by dynamic contrast susceptibility imaging (DSC) in pediatric patients with MMD [10]. However, a previous study of carotid artery stenosis did not find a correlation between OEF and ASL-CoV [9]. Additionally, to the best of our knowledge, no previous study has reported the relationship between ASL-CoV and OEF in patients with MMD.

Because the MTT measured by DSC can be used to detect an increased OEF [11] and ASL-CoV correlates with time-based parameters such as the MTT [9, 10], we hypothesized that ASL-CoV of a single PLD can detect hemodynamic disturbance measured with PET, especially the status of an increased OEF in adult patients with MMD. Because ASL is strongly affected by the ATT [4], the ATT of the evaluated ROI and PLD may affect the ASL-CoV values and the ability to detect hemodynamic disturbance. Therefore, the purpose of this study is (1) to evaluate the differences in ASL-CoV among regions within MCA areas using ATT-based flow territories [12] and two PLDs, (2) to evaluate the correlation between ASL-CoV and PET-measured hemodynamic parameters and compare them with the correlation between ASL-CBF and PET parameters, and (3) to investigate the diagnostic ability of ASL-CoV to detect increased OEF.

Material and methods

This retrospective study was approved by the ethics committee of the local institute. In our institute, ASL has been acquired in all MRI studies upon initial evaluation and during follow-up for adult patients with MMD since April 2011, when the scanner was introduced at our institute. We only perform PET when a hemodynamic disturbance is suspected by perfusion MRI [7, 11, 13], and further evaluation is required to detect the presence of misery perfusion, which is a surgical indication at our institute. The inclusion criteria of this study were as follows: (1) a diagnosis of MMD according to the diagnostic guidelines [14], (2) no surgical treatments before the imaging studies, (3) no infarction or hemorrhage in the cortex affecting spatial normalization and regional value analysis observed on routine MRI, (4) ASL and PET both performed from April 2011 to August 2020, < 60 days apart [15], and (5) no new lesions or symptoms between the ASL and PET

studies. From a review of medical records and the scanner examination list, 68 patients who satisfied the inclusion criteria were identified. A summary of the patients' characteristics is given in Table 1.

ASL acquisition

Using a 3.0-T MR scanner (GE Signa HDxt; GE Healthcare, Waukesha, WI) with an eight-channel head coil, three-dimensional pseudocontinuous ASL images were acquired using the following parameters: repetition time, 4521 ms; echo time, 9.812 ms; field of view, 24 cm; 512 sampling points on eight spirals (matrix size, 512 × 8); voxel size, 1.88 × 1.88 × 4.0 mm³; number of slices, 30; number of excitations, 3; bandwidth, 62.50 Hz; and labeling time, 1.5 s. PLDs of 1525 ms and 2525 ms were chosen to cover both pediatric and adult patients [4], respectively, with the same protocol and as a tradeoff between using a long PLD to cover transit delays (a longer PLD provides a more accurate CBF [16]) and the signal-to-noise ratio (a longer PLD in our clinical scanner results in poor image quality). A vascular crush gradient was not applied because arterial transit artifacts themselves suggest hemodynamic disturbances in patients with MMD [13, 17]. The quantitative ASL-CBF map was generated on an Advantage Windows workstation using Functool software attached to the scanner [18]. The acquisition time of each ASL image was 4 min 22 s and 5 min 3 s, and the total acquisition time of each MRI protocol, including magnetic resonance angiography, fluid-attenuated inversion recovery imaging, T2-weighted imaging, and T2*-weighted imaging, was approximately 30 min.

Table 1 Summary of patient backgrounds. *SD*, standard deviation; *TIA*, transient ischemic attack; *MRA*, magnetic resonance angiography; *Lt*, left; *Right*, right; *NA*, not available

		(n = 68)
Age (mean ± SD, range)		39.4 ± 9.3 (20–61)
Sex (no. of females)		52 (76.7%)
Clinical presentation	TIA	34 (50.0%)
	TIA + infarction	3 (4.4%)
	Infarction	6 (8.8%)
	Hemorrhage	8 (11.8%)
MRA stage (no. of 1/2/3/4)	Lt	6/18/38/6
	Rt	9/14/34/11
<i>RNF213</i> p.R4810K variant	Heterozygous	47 (69.1%)
	Wild	6 (8.8%)
	NA	15 (22.1%)
Subsequent treatment	Revascularization surgery	40 (58.8%)
	Conservative	28 (41.2%)

PET acquisition

The ^{15}O -gas PET study was performed using two scanners: a HEADTOME-V system (Shimadzu, Kyoto, Japan) until March 2013 ($n = 13$) and a Discovery 710 PET/CT system (GE Healthcare, Milwaukee, WI, USA) thereafter ($n = 55$), following a scanner update. Full details are presented in the Supplemental Methods of the Supplementary information. Briefly, the ^{15}O -gas PET study included three emission scans performed sequentially with short inhalations of C^{15}O , $^{15}\text{O}_2$, and C^{15}O_2 . CBF, cerebral blood volume (CBV), and OEF maps were calculated by continuous arterial blood sampling using a table lookup technique [19, 20]. The regional CBF and OEF values were corrected for delay and dispersion [21], and the regional OEF values were further corrected for the effect of the regional CBV [22, 23].

Image analysis and calculation of regional values

Region of interest (ROI) analysis was performed between the ASL-CoV and PET parameters in middle cerebral artery (MCA) areas, which constitute the main affected vascular region in this disease [6] and the main target of revascularization surgery [1], by an automated algorithm that could be performed for each patient in clinical settings in the MATLAB 2019b environment (The MathWorks Inc., Natick, MA). The ASL-CBF (PLD = 1525 ms) and PET-CBF maps of each subject were spatially normalized to Montreal Neurological Institute space to obtain an isotropic voxel size of 2 mm using SPM12 (<http://www.fil.ion.ucl.ac.uk/spm>). The same transformation matrix used for the ASL-CBF (PLD = 1525 ms) map/the PET-CBF map was applied to the ASL-CBF (PLD = 2525 ms) map/the remaining PET maps of each patient. The accuracy of the spatial normalization was visually confirmed for each map. To eliminate the extremely high signals produced by large veins and sinuses in the CBV map, the top 40% of all voxel values were deleted from each CBV map, with the threshold empirically determined to delete large veins but not parenchymal signals. Then, the average value of each of the parameters of the bilateral proximal, middle, and distal MCA areas [12] (Fig. 1) and the cerebellum [24] was measured using the distributed territorial atlas (ATTbasedFlowTerritories.nii, https://figshare.com/articles/dataset/ATT_based_flow_territories/1488674). The SD of ASL (ASL-SD) within each region was also obtained, and ASL-CoV of each area was calculated by dividing the SD by the average regional value (i.e., ASL-SD/ASL-CBF) [8]. MTT was calculated by dividing the CBV by the CBF. Because we used two PET scanners with different acquisition methods, all regional PET values were normalized to the values of the cerebellum.

Statistical analysis

Statistical analysis was performed using JMP version 12.0.1 (SAS Institute, Cary, NC), and $P < 0.05$ (with or without multiple comparisons for two ASLs/three regions) was regarded as statistically significant. First, the normality of the distribution of each value was evaluated by the Shapiro–Wilk test. Each subsequent analysis was performed using 136 regional values (including both the right and left sides) from 68 patients.

The ASL-CBF and ASL-CoV values in each region (proximal, middle, and distal MCA) were evaluated by the two-sided Jonckheere–Terpstra trend test to evaluate whether there was an increasing or decreasing trend for each of the regions and by the Steel–Dwass test to investigate the differences among each region. The differences between ASL-CBF and ASL-CoV for PLD = 1525 ms and PLD = 2525 ms were assessed using a Wilcoxon signed-rank test. Post hoc power analysis was performed using G*Power ver. 3.1.9.7 [25].

The correlations between ASL-CBF, ASL-CoV, and PET parameters in each region were calculated using Spearman correlation coefficients and tested for significance. The differences among correlation coefficients were calculated and tested for significance using Fisher's Z transformation. The strength of the correlations was described using the Evans classification [26].

The ASL-CoV values of regions with an increased OEF (OEF ratio > 1.13 [27]) or a nonincreased OEF (OEF ratio ≤ 1.13) were compared by a Wilcoxon signed-rank test. The sensitivity, specificity, negative predictive value, and positive predictive value of the ASL-CoV and the cutoff value, as well as the area under the receiver operating characteristic curve, were calculated for each region and PLD.

The full dataset is available from the corresponding author upon reasonable request.

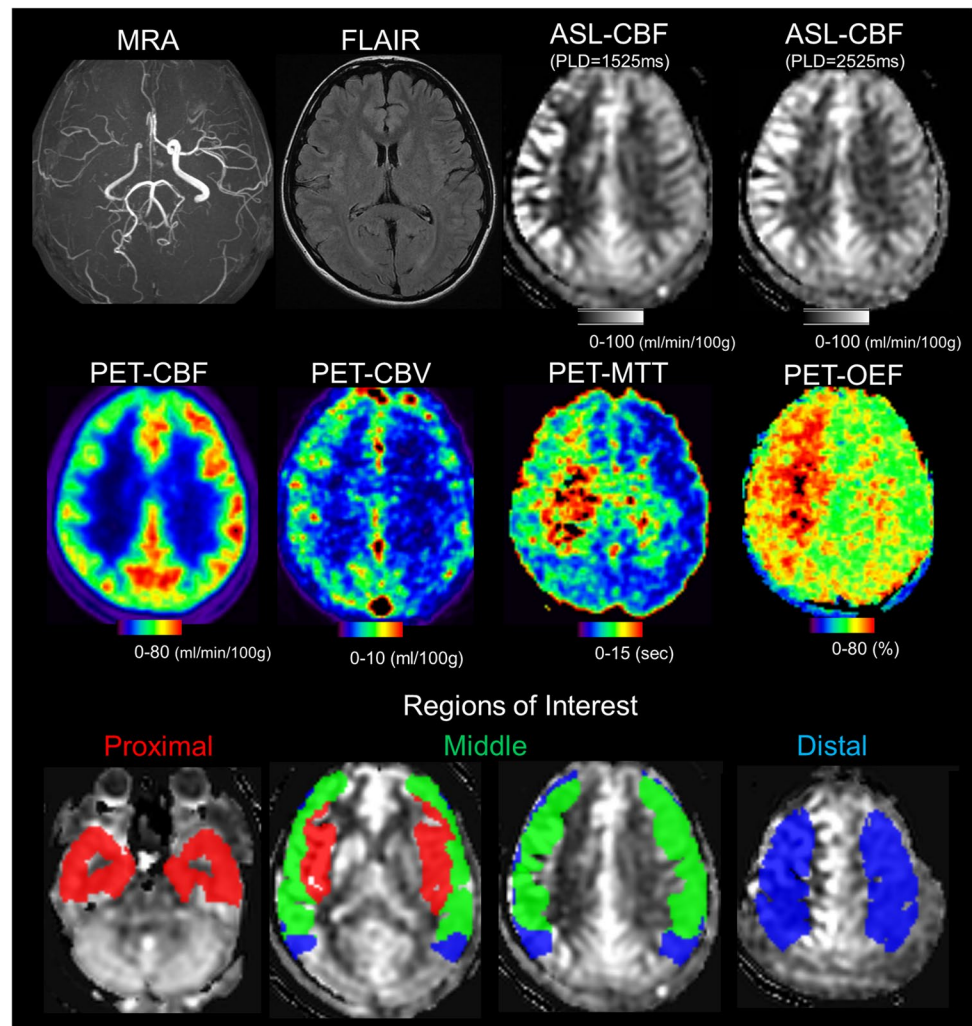
Results

Representative parametric maps and ROIs used in this study are shown in Fig. 1. None of the calculated values was normally distributed ($P < 0.001$); therefore, nonparametric analysis was applied in all subsequent steps.

ASL-CBF and ASL-CoV values in ATT-based flow territories

ASL-CBF values showed a significant decreasing trend for both PLDs (Fig. 2, $P < 0.001$), and distal regions showed significantly lower values than proximal and middle regions. In any region, the values of ASL-CBF (PLD = 1525 ms) were lower than those of ASL-CBF (PLD = 2525 ms; $P < 0.001$).

Fig. 1 Representative parametric maps from a 20-year-old female who presented with transient left-sided hemiparesis. Magnetic resonance angiography (MRA) shows occlusion of the internal carotid artery, and fluid-attenuated inversion recovery (FLAIR) imaging shows an ivy sign on the right hemisphere but no parenchymal lesions. The right hemisphere shows arterial transit artifacts on the cerebral blood flow map of arterial spin labeling (ASL-CBF) and contains more voxels with low signals with a postlabeling delay (PLD) of 1525 ms than with a PLD of 2525 ms. Parametric maps of positron emission tomography (PET) maps show typical misery perfusion on the same side (i.e., a decreased CBF and an increased cerebral blood volume (CBV), mean transit time (MTT), and oxygen extraction fraction (OEF))



ASL-CoV showed a significant increasing trend for both PLDs (Fig. 2, $P < 0.001$), with distal regions showing the lowest ASL-CBF and highest ASL-CoV values for both PLDs. In any region, the ASL-CoV values for PLD = 1525 ms were higher than those for PLD = 2525 ms ($P < 0.001$).

Correlations of ASL-CBF, ASL-CoV, and PET parameters

The correlations between ASL-CBF and PET parameters were different among regions and parameters (Fig. 3, upper parts). In the correlation between ASL-CBF and PET-CBF, the correlation coefficient in the distal region was better than that in the proximal and middle regions, and the correlation was significantly better for ASL-CBF (PLD = 1525 ms) than for ASL-CBF (PLD = 2525 ms; $P = 0.03$). Using either PLD, the correlation of ASL-CBF with PET-CBV or PET-MTT in the proximal region was positive and opposite the correlation in the middle and distal regions. The correlation

between ASL-CBF and PET-OEF was moderate in the middle and distal regions when using PLD = 1525 ms and weak when using PLD = 2525 ms.

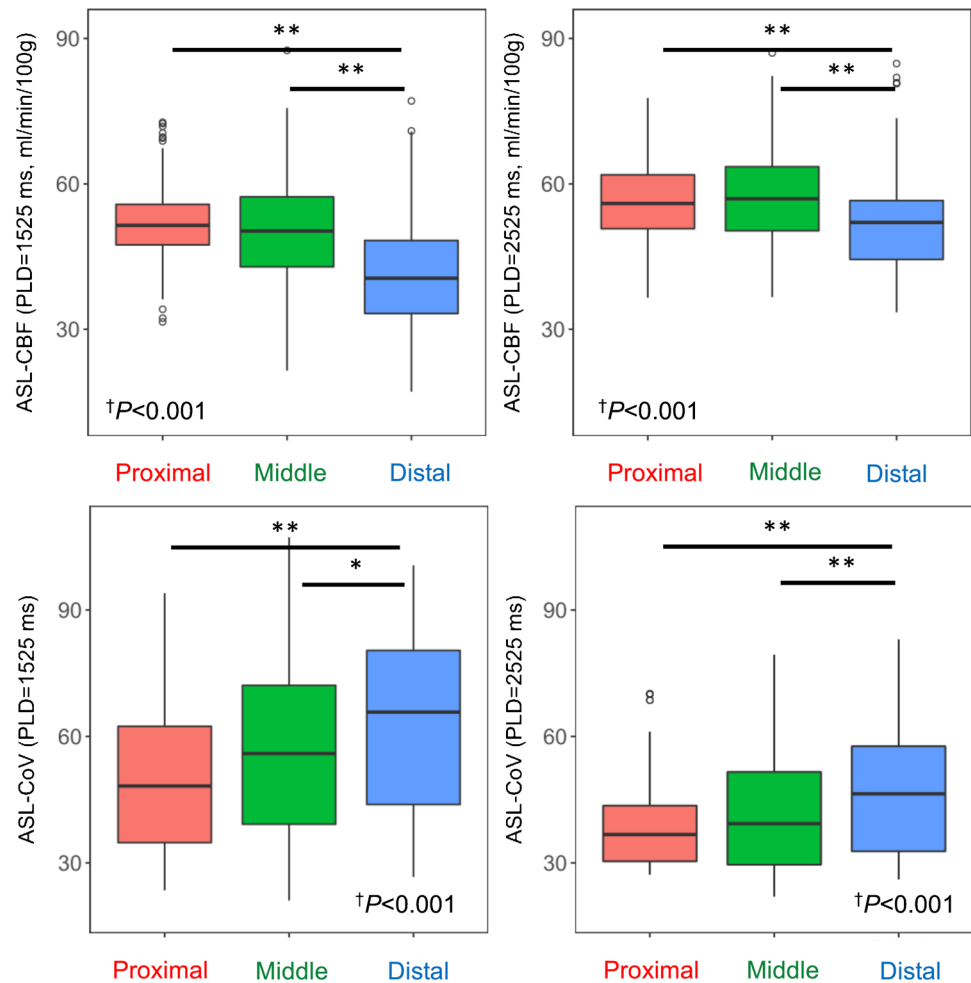
The ASL-CoV values showed moderate to strong correlations with the PET parameters, including PET-OEF, for both PLDs and all regions, and none was significantly different from the others ($P > 0.05$, Fig. 3, lower parts). The correlation coefficient was higher for PET-CBV and PET-MTT than that for PET-CBF and PET-OEF, but the difference was not significant ($P > 0.05$).

Post hoc analysis revealed that the actual statistical power of all correlation analyses was > 0.95 .

ASL-CoV and an increased OEF with two PLDs and in ATT-based flow territories

The number and percentage of regions with an increased OEF were 39 (28.7%), 76 (55.9%), and 83 (61.0%) in proximal, middle, and distal regions, respectively. The ASL-CoV values of regions with an increased OEF were significantly

Fig. 2 ASL-CBF and ASL-CoV values in the proximal, middle, and distal MCA regions. A significant ($P < 0.001$) decreasing trend for ASL-CBF and an increasing trend for ASL-CoV were observed for both post-labeling delays (PLDs). Both ASL-CBF and ASL-CoV in the distal region are significantly different from those in the proximal and middle regions. † $P < 0.001$ (Jonckheere-Terpstra trend test), * $P < 0.05$ (Steel–Dwass test), and ** $P < 0.05$ (Steel–Dwass test, corrected for multiple comparisons for two PLDs/three regions)



higher than the values of regions with a nonincreased OEF with either PLD or in any region (Fig. 4, upper column). The area under the curve was highest when using a PLD of 1525 ms in the middle regions (Fig. 4, lower column and Table 2). When using ASL-CoV measured with a PLD of 1525 ms in middle regions with a cutoff value of 31.27, the sensitivity and the negative predictive value were the highest (Table 2).

Discussion

By using ATT flow-based ROIs and two PLDs, we found that the ASL-CoV and ASL-CBF values were strongly affected by the choice of ROI and PLD, and ASL-CoV was highest, and ASL-CBF was lowest in distal regions using a short PLD. By definition, the ASL-CoV value (ASL-SD/ASL-CBF) increases as the ASL-CBF value decreases; therefore, more affected regions with low true CBF values and apparently low ASL-CBF values as an effect of perfusion delay [7] will result in higher ASL-CoV values. The ASL-CBF values were lower in distal regions using the shorter PLD,

which can explain the regional and PLD differences in ASL-CoV values. Again, by definition, the ASL-CoV values also increased as the SD within the ROI increased, but the differences in the SD among regions were not as prominent as those of the ASL-CBF and ASL-CoV values (Supplemental Fig. 1 in Supplementary information). Considering the weak increasing trend in ASL-SD when using a PLD of 2525 ms, ASL-SD might contribute to higher ASL-CoV values in distal regions when using a PLD of 2525 ms. Nevertheless, regional and PLD differences in ASL-CoV values must mainly reflect the regional and PLD differences in ASL-CBF rather than ASL-SD.

In the proximal region, the correlation between ASL-CBF and PET-CBF was poor, and the correlation between ASL-CBF and PET-CBV or PET-MTT was opposite to the correlation in the middle and distal regions for the short PLD. Theoretically, the proximal region has a shorter ATT than the middle and distal regions, so the ASL-CBF values should be close to the true CBF values measured with PET, in contrast to the observed results. As arterial stenosis progresses and the ATT increases, ASL-CBF will decrease, and PET-CBV or PET-MTT will increase; thus, the correlation

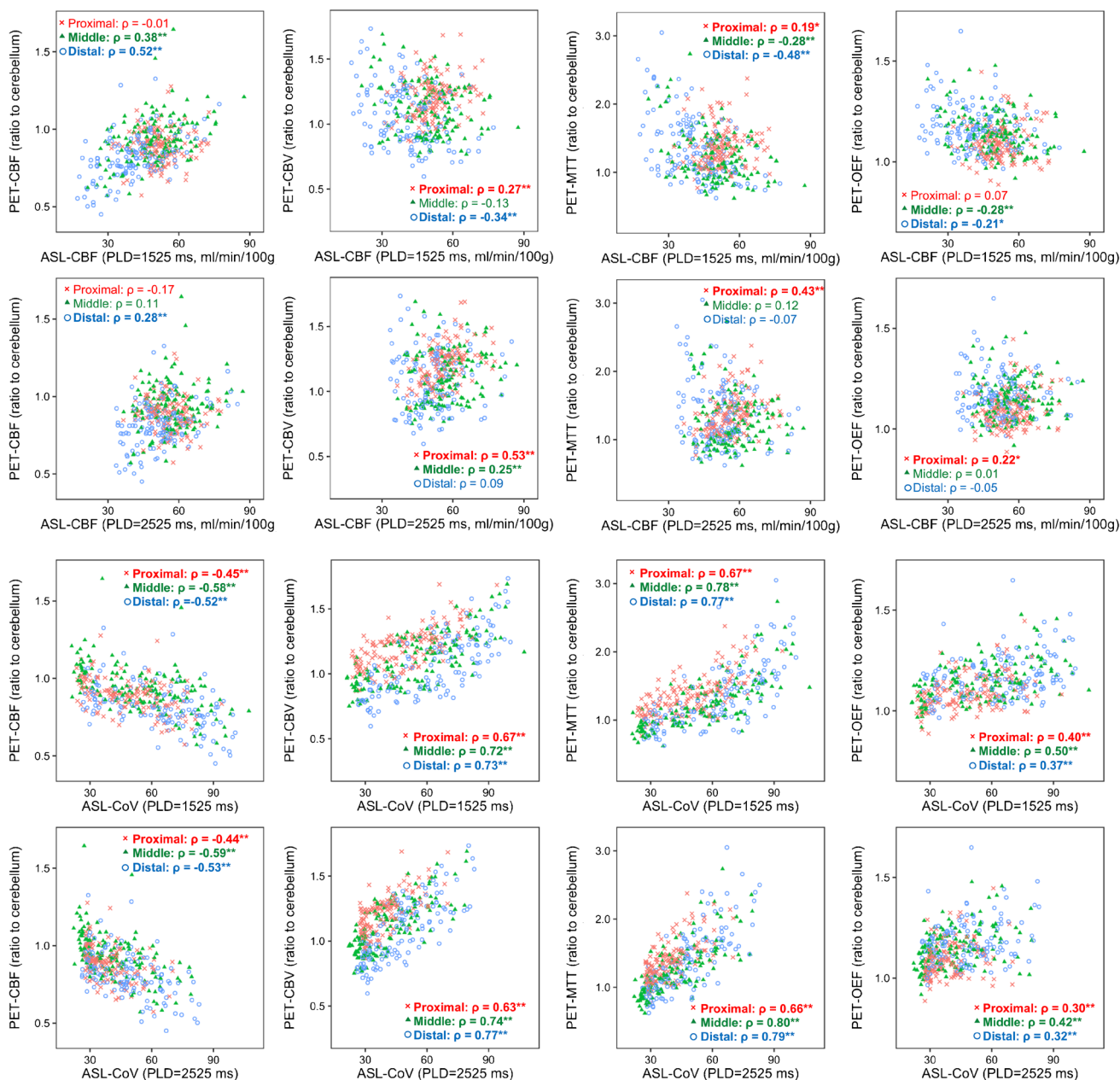


Fig. 3 Correlation between ASL-CBF, ASL-CoV, and PET parameters in the proximal, middle, and distal MCA regions. The correlations between ASL-CBF and the PET parameters are significant and moderate in selected regions but are generally weak. On the other hand, ASL-CoV shows a moderately significant correlation with PET parameters, including the OEF, for both ASLs and all regions. The

correlation coefficient was higher in the middle region than in the proximal and distal regions in all analyses, but the differences were not statistically significant. PLD, postlabeling delay. * $P < 0.05$ and ** $P < 0.05$ (corrected for multiple comparisons for two PLDs/three regions)

between ASL-CBF and PET-CBV should be negative, which was also opposite the observation in the proximal regions. Perhaps the increased CBV that reflects leptomenigeal anastomosis and vasodilation observed in asymptomatic to symptomatic patients with MMD [2] affects the ASL-CBF values by increasing arterial transit artifacts [13] and causes the ASL-CBF value to be higher than the values in areas

without CBV elevation. The overestimation effect of the CBV on ASL-CBF might attenuate the correlation between ASL-CBF and PET-CBF in the proximal region, resulting in a paradoxically positive correlation between ASL-CBF and PET-CBV. The effect of an increased CBV on the ASL-CBF value seemed small in the distal area when using a short PLD, possibly because the ATT was longer than the PLD,

Fig. 4 Relationship between ASL-CoV and an increased oxygen extraction fraction (OEF) in the proximal, middle, and distal MCA regions. Regardless of the choice of PLD and regions, the ASL-CoV values of regions with an increased OEF were significantly higher than those of regions with a nonincreased OEF (upper column). The receiver operating characteristic curve analysis of ASL-CoV showed that the area under the curve (AUC) was the highest when using a PLD of 1525 ms in middle regions. * $P < 0.05$ and ** $P < 0.05$ (corrected for multiple comparisons for two PLDs/three regions)

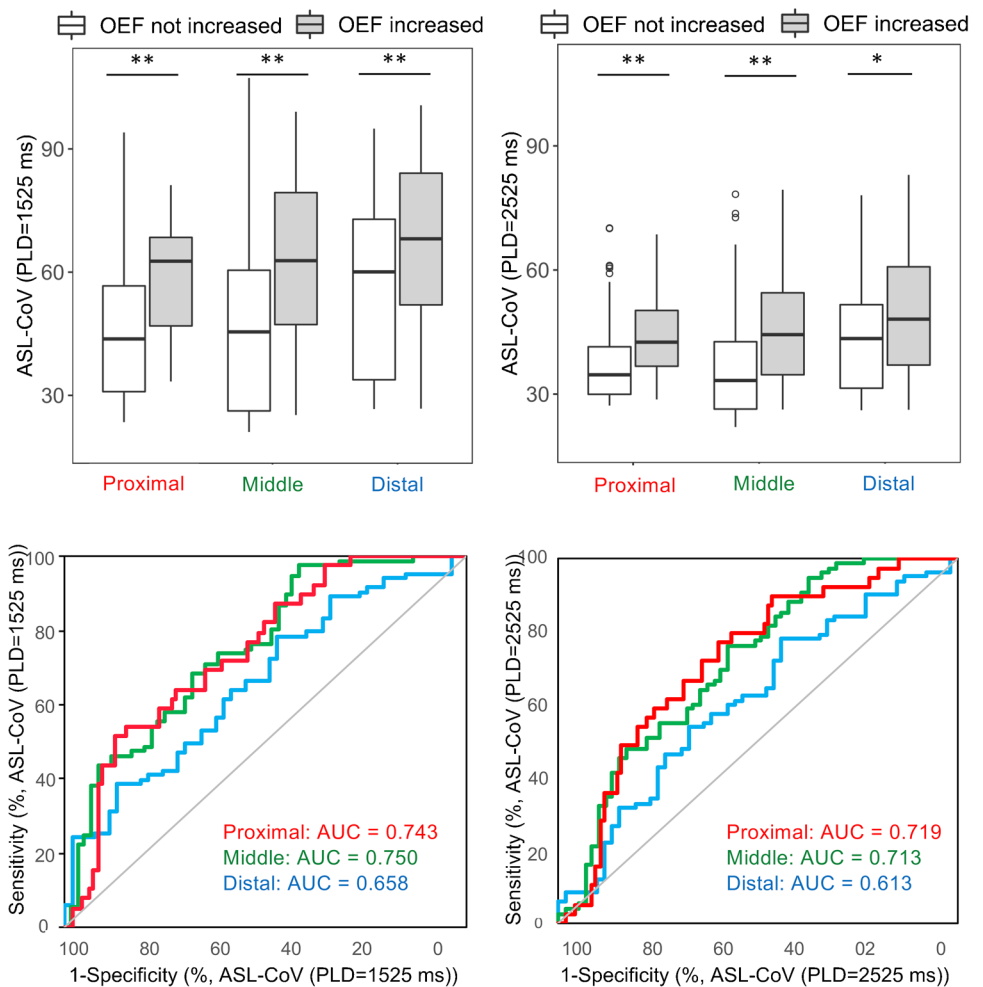


Table 2 Receiver operating curve analysis of ASL-CoV to detect an increased oxygen extraction fraction (OEF)

		AUC	ASL-CoV cutoff value	Sensitivity (%)	Specificity (%)	NPV (%)	PPV (%)
ASL-CoV (PLD = 1525 ms)	Proximal	0.743	62.67	51.3	87.6	81.7	62.5
	Middle	0.750	31.27	97.4	41.7	92.6	67.9
	Distal	0.658	50.88	78.3	47.2	58.1	69.9
ASL-CoV (PLD = 2525 ms)	Proximal	0.719	36.69	76.9	60.0	86.4	44.1
	Middle	0.713	34.61	76.0	57.6	65.4	69.5
	Distal	0.613	35.83	78.1	44.3	56.1	68.8

The highest value of each parameter (except for the cutoff value) is shown in bold. *PLD*, postlabeling delay; *AUC*, area under the curve; *NPV*, negative predictive value; *PPV*, positive predictive value

and few labeled protons arrived at the ROIs. If we obtain ASL-CBF using a longer PLD, the distal area might also have a positive correlation with PET-CBV. The true effect of the CBV on the ASL-CBF value can be clarified if the CBV alone can be increased under physiological conditions, which is difficult in reality because the use of vasodilator agents to increase the CBV simultaneously shortens the transit time [28].

Regardless of the choice of the ROI and PLD, ASL-CoV showed a moderate to strong correlation with the PET parameters, while the correlation of ASL-CBF varied depending on the ROI and PLD. As discussed above, ASL-CBF values can underestimate true CBF values due to the elongated ATT, while they can also overestimate true CBF owing to arterial transit artifacts. Correlations with ASL-CBF and PET parameters may be better in distal regions

when using short PLDs because the effect of overestimation from arterial transit artifacts is small. In other regions and with long PLDs, a mixture of both overestimation and underestimation might lead to poor correlations. On the other hand, ASL-SD values that capture intraregional variation might be more sensitive to hemodynamic disturbance, as ASL-SD values in most regions showed better correlations with PET parameters than ASL-CBF values, except for distal regions using a short PLD (Supplemental Fig. 2 in Supplementary information). Upon dividing ASL-SD by ASL-CBF, ASL-CoV may increase as hemodynamic disturbance becomes more severe and correlates well with PET-measured parameters regardless of the choice of ROI and PLD.

We found that ASL-CoV was better correlated with PET-CBV and PET-MTT than PET-CBF and PET-OEF, although the correlation was not statistically significant. One reason might be that CBV and MTT values start to increase in the early stage of hemodynamic disturbance (Power's Stage 1), while CBF and OEF are not affected until the hemodynamic disturbance becomes severe (Power's Stage 2). Another reason might be the increased CBV as the prominent feature of MMD compared to atherosclerotic cerebrovascular disease [29]. A previous study in patients with carotid artery stenosis showed that ASL-CoV correlated with CBF and MTT but not with CBV [9]. The correlation between ASL-CoV and MTT in this study was similar to the reported correlation between ASL-CoV and a time-based parameter in pediatric patients with MMD ($r=0.51-0.82$).

We found a significant correlation between ASL-CoV and OEF in our patients with MMD, while a previous study evaluating patients with carotid artery stenosis reported a negative correlation between them [9]. We believe that this difference comes from the number of ROIs with increased OEF. In a previous study evaluating patients with carotid artery stenosis, the ipsilesional OEF did not significantly differ from contralateral OEF values, which suggests that the number of patients showing an increased OEF was small. In contrast, many regions showed an increased OEF in each ROI, partly because we only performed PET in patients with a suspected increased OEF, and the variety of OEF values might have led to the significant correlation between ASL-CoV and the OEF. This difference may also be due to inter-patient variation in the degree of hemodynamic disturbance in patients with MMD [2]. Nevertheless, as stated above, the correlation with ASL-CoV was better for the MTT than for the OEF, and it may be difficult to detect an increased OEF by simple correlation analysis with ASL-CoV.

Although the correlation between the ASL-CoV and PET parameters was significant regardless of the choice of the PLD and ROI, the diagnostic ability to identify an increased OEF seemed better when using a PLD of 1525 ms, especially in the middle region. Perhaps a PLD of 1525 ms is

better than a PLD of 2525 ms because the heterogeneity of the voxel values is emphasized by arterial transit artifacts and hypoperfused areas with shorter PLDs. The middle region might be better than the proximal and distal regions, as the balance between the overestimation effect due to arterial transit artifacts (strong in the proximal region) and the underestimation effect due to an elongated ATT (strong in the distal region) and the higher heterogeneity of voxel values within ROIs lead to a wide range of ASL-CoV values in the middle region compared to the proximal and distal regions (Fig. 2). Unfortunately, current data regarding ASL-CoV are unsatisfactory for directly detecting an increased OEF, which is a biomarker of misery perfusion, and it cannot serve as a total substitute for ^{15}O -gas PET imaging, as shown in a study using dynamic contrast susceptibility imaging [11]. However, considering the high sensitivity and negative predictive value, ASL-CoV measured with a single PLD of 1525 ms might be used to exclude patients without increased OEF in the middle region.

Limitations of this study include the retrospective nature with a relatively long interval between MRI and PET studies, which was inevitable because both studies were acquired not for research but for clinical purposes and because of a lack of PET/MR scanners in our institute. Because only patients with suspected hemodynamic disturbance on MR perfusion were included, there is substantial selection bias; however, the inclusion of patients with less affected hemodynamics (i.e., regions with lower ASL-CoV, PET-CBV, PET-MTT, and PET-OEF values and higher PET-CBF values) will only improve the correlations; and thus, the good correlations observed without including less affected patients suggest that the strong correlations between the ASL-CoV and PET parameters are genuine. We did not acquire ASL for PLD = 2000 ms, which is the currently recommended PLD for adult patients according to an expert consensus paper [4] due to the reasoning described in the "Methods" section. Because we only acquired ASL using two PLDs, we did not directly measure the ATT, which will likely correlate well with ASL-CoV [9]. ASL-CoV calculated from another ASL technique might be better than pseudocontinuous ASL [30]. Anatomical MRI data for eliminating the partial volume effect and data from normal volunteers were lacking.

Although limitations exist, this is a unique study showing that although ASL-CoV values are affected by ATT-flow-based ROIs and the choice of PLD, ASL-CoV measured with a single PLD correlated with PET-measured hemodynamic parameters in patients with MMD and may help identify patients with increased OEF. If ASL-CoV measured with a single PLD of 1525 ms can be used to estimate the hemodynamic disturbance measured with PET, we can shorten the scanning time and use ASL-CoV as the reference to determine the need for invasive PET imaging studies for individual patients.

Supplementary Information The online version contains supplementary material available at <https://doi.org/10.1007/s00234-021-02802-y>.

Acknowledgements We thank Ryotaro Sakakibara for helping post-process the images.

Funding This work was supported by the Grants-in-Aid for Scientific Research “KAKENHI,” the Japan Society for the Promotion of Science (Grant #24592115), and a research grant (2015–2017) from the Japanese Society of Neuroradiology, both of which are given to Yoji Tanaka. For the remaining authors, none was declared.

Data availability The full dataset is available from the corresponding author upon reasonable request.

Code availability The MATLAB code used in this study is available from the corresponding author upon reasonable request.

Declarations

Conflict of interest The authors declare that they have no conflict of interest.

Ethical approval All procedures performed in the studies involving human participants were in accordance with the ethical standards of the institutional and/or national research committee and with the 1964 Helsinki Declaration and its later amendments or comparable ethical standards.

Informed consent Informed consent was obtained from all individual participants included in the study.

Consent to participate Informed consent was obtained from all participants.

Consent for publications Additional informed consent was obtained from all individual participants for whom identifying information was included in this article.

References

- Kuroda S, Houkin K (2008) Moyamoya disease: current concepts and future perspectives. *Lancet Neurol* 7(11):1056–1066. [https://doi.org/10.1016/s1474-4422\(08\)70240-0](https://doi.org/10.1016/s1474-4422(08)70240-0)
- Nariai T, Matsushima Y, Imae S, Tanaka Y, Ishii K, Senda M, Ohno K (2005) Severe haemodynamic stress in selected subtypes of patients with moyamoya disease: a positron emission tomography study. *J Neurol Neurosurg Psychiatry* 76(5):663–669. <https://doi.org/10.1136/jnnp.2003.025049>
- Powers WJ, Grubb RL Jr, Raichle ME (1984) Physiological responses to focal cerebral ischemia in humans. *Ann Neurol* 16(5):546–552. <https://doi.org/10.1002/ana.410160504>
- Alsop DC, Detre JA, Golay X, Gunther M, Hendrikse J, Hernandez-Garcia L, Lu H, MacIntosh BJ, Parkes LM, Smits M, van Osch MJ, Wang DJ, Wong EC, Zaharchuk G (2015) Recommended implementation of arterial spin-labeled perfusion MRI for clinical applications: a consensus of the ISMRM perfusion study group and the European consortium for ASL in dementia. *Magn Reson Med* 73(1):102–116. <https://doi.org/10.1002/mrm.25197>
- Puig O, Henriksen OM, Vestergaard MB, Hansen AE, Andersen FL, Ladefoged CN, Rostrup E, Larsson HB, Lindberg U, Law I (2020) Comparison of simultaneous arterial spin labeling MRI and (15)O-H₂O PET measurements of regional cerebral blood flow in rest and altered perfusion states. *J Cereb Blood Flow Metab* 40(8):1621–1633. <https://doi.org/10.1177/0271678X19874643>
- Fan AP, Khalighi MM, Guo J, Ishii Y, Rosenberg J, Wardak M, Park JH, Shen B, Holley D, Gandhi H, Haywood T, Singh P, Steinberg GK, Chin FT, Zaharchuk G (2019) Identifying hypoperfusion in moyamoya disease with arterial spin labeling and an [¹⁵O]-water positron emission tomography/magnetic resonance imaging normative database. *Stroke* 50(2):373–380
- Hara S, Tanaka Y, Ueda Y, Hayashi S, Inaji M, Ishiwata K, Ishii K, Maehara T, Nariai T (2017) Noninvasive evaluation of CBF and perfusion delay of moyamoya disease using arterial spin-labeling MRI with multiple postlabeling delays: comparison with 15O-Gas PET and DSC-MRI. *AJNR Am J Neuroradiol* 38(4):696–702. <https://doi.org/10.3174/ajnr.A5068>
- Mutsaerts HJ, Petr J, Vaclavu L, van Dalen JW, Robertson AD, Caan MW, Masellis M, Nederveen AJ, Richard E, MacIntosh BJ (2017) The spatial coefficient of variation in arterial spin labeling cerebral blood flow images. *J Cereb Blood Flow Metab* 37(9):3184–3192. <https://doi.org/10.1177/0271678x16683690>
- Ibaraki M, Nakamura K, Toyoshima H, Takahashi K, Matsubara K, Umetsu A, Pfeuffer J, Kuribayashi H, Kinoshita T (2019) Spatial coefficient of variation in pseudo-continuous arterial spin labeling cerebral blood flow images as a hemodynamic measure for cerebrovascular steno-occlusive disease: a comparative (15)O positron emission tomography study. *J Cereb Blood Flow Metab* 39(1):173–181. <https://doi.org/10.1177/0271678x18781667>
- Tortora D, Scavetta C, Rebella G, Bertamino M, Scala M, Giacomini T, Morana G, Pavanello M, Rossi A, Severino M (2020) Spatial coefficient of variation applied to arterial spin labeling MRI may contribute to predict surgical revascularization outcomes in pediatric moyamoya vasculopathy. *Neuroradiology* 62(8):1003–1015. <https://doi.org/10.1007/s00234-020-02446-4>
- Tanaka Y, Nariai T, Nagaoka T, Akimoto H, Ishiwata K, Ishii K, Matsushima Y, Ohno K (2006) Quantitative evaluation of cerebral hemodynamics in patients with moyamoya disease by dynamic susceptibility contrast magnetic resonance imaging—comparison with positron emission tomography. *J Cereb Blood Flow Metab* 26(2):291–300. <https://doi.org/10.1038/sj.jcbfm.9600187>
- Mutsaerts HJ, van Dalen JW, Heijtel DF, Groot PF, Majoie CB, Petersen ET, Richard E, Nederveen AJ (2015) Cerebral perfusion measurements in elderly with hypertension using arterial spin labeling. *PLoS ONE* 10(8):e0133717. <https://doi.org/10.1371/journal.pone.0133717>
- Hara S, Tanaka Y, Ueda Y, Abe D, Hayashi S, Inaji M, Maehara T, Ishii K, Nariai T (2020) Detection of hemodynamic impairment on (15)O gas PET using visual assessment of arterial spin-labeling MR imaging in patients with moyamoya disease. *J Clin Neurosci* 72:258–263. <https://doi.org/10.1016/j.jocn.2019.11.026>
- Tominaga T, Suzuki N, Miyamoto S, Koizumi A, Kuroda S, Takahashi JC, Fujimura M, Houkin K (2018) Recommendations for the management of moyamoya disease: a statement from research committee on spontaneous occlusion of the circle of willis (moyamoya disease) [2nd Edition]. *Surg Cereb Stroke* 46(1):1–24. <https://doi.org/10.2335/scs.46.1>
- Hara S, Tanaka Y, Hayashi S, Inaji M, Maehara T, Hori M, Aoki S, Ishii K, Nariai T (2019) Bayesian estimation of CBF measured by DSC-MRI in patients with moyamoya disease: comparison with (15)O-gas pet and singular value decomposition. *AJNR Am J Neuroradiol* 40(11):1894–1900. <https://doi.org/10.3174/ajnr.A6248>
- Fan AP, Guo J, Khalighi MM, Gulaka PK, Shen B, Park JH, Gandhi H, Holley D, Rutledge O, Singh P, Haywood T, Steinberg GK, Chin FT, Zaharchuk G (2017) Long-delay arterial spin labeling

- provides more accurate cerebral blood flow measurements in moyamoya patients: a simultaneous positron emission tomography/mri study. *Stroke* 48(9):2441–2449. <https://doi.org/10.1161/strokeaha.117.017773>
17. Zaharchuk G, Do HM, Marks MP, Rosenberg J, Moseley ME, Steinberg GK (2011) Arterial spin-labeling MRI can identify the presence and intensity of collateral perfusion in patients with moyamoya disease. *Stroke* 42(9):2485–2491. <https://doi.org/10.1161/STROKEAHA.111.616466>
 18. Ye FQ, Berman KF, Ellmore T, Esposito G, Horn JDv, Yang Y, Duyn J, Smith AM, Frank JA, Weinberger DR, McLaughlin AC (2000) H215O PET validation of steady-state arterial spin tagging cerebral blood flow measurements in humans. *Magn Reson Med* 44:450–456
 19. Senda M, Buxton RB, Alpert NM, Correia JA, Mackay BC, Weise SB, Ackerman RH (1988) The 15O steady-state method: correction for variation in arterial concentration. *J Cereb Blood Flow Metab* 8(5):681–690. <https://doi.org/10.1038/jcbfm.1988.115>
 20. Sadato N, Yonekura Y, Senda M, Iwasaki Y, Matoba N, Tamaki N, Sasayama S, Magata Y, Konishi J (1993) PET and the autoradiographic method with continuous inhalation of oxygen-15-gas: theoretical analysis and comparison with conventional steady-state methods. *J Nucl Med* 34(10):1672–1680
 21. Iida H, Kanno I, Miura S, Murakami M, Takahashi K, Uemura K (1986) Error analysis of a quantitative cerebral blood flow measurement using H2(15)O autoradiography and positron emission tomography, with respect to the dispersion of the input function. *J Cereb Blood Flow Metab* 6:536–545
 22. Mintun MA, Raichle ME, Martin WR, Herscovitch P (1984) Brain oxygen utilization measured with O-15 radiotracers and positron emission tomography. *J Nucl Med* 25(2):177–187
 23. Lammertsma AA, Jones T (1983) Correction for the presence of intravascular oxygen-15 in the steady-state technique for measuring regional oxygen extraction ratio in the brain: 1. Description of the method. *J Cereb Blood Flow Metab* 3(4):416–424. <https://doi.org/10.1038/jcbfm.1983.67>
 24. Mazziotta J, Toga A, Evans A, Fox P, Lancaster J, Zilles K, Woods R, Paus T, Simpson G, Pike B, Holmes C, Collins L, Thompson P, MacDonald D, Iacoboni M, Schormann T, Amunts K, Palomero-Gallagher N, Geyer S, Parsons L, Narr K, Kabani N, Le Goualher G, Boomsma D, Cannon T, Kawashima R, Mazoyer B (2001) A probabilistic atlas and reference system for the human brain: international consortium for brain mapping (ICBM). *Philos Trans R Soc Lond B Biol Sci* 356(1412):1293–1322. <https://doi.org/10.1098/rstb.2001.0915>
 25. Faul F, Erdfelder E, Lang AG, Buchner A (2007) G*Power 3: a flexible statistical power analysis program for the social, behavioral, and biomedical sciences. *Behav Res Methods* 39(2):175–191
 26. Evans JD (1996) Straightforward statistics for the behavioral sciences. Brooks/Cole Publishing, Pacific Grove
 27. Reynolds MR, Grubb RL Jr, Clarke WR, Powers WJ, Zipfel GJ, Adams HP Jr, Derdeyn CP, Carotid Occlusion Surgery Study Investigators (2013) Investigating the mechanisms of perioperative ischemic stroke in the carotid occlusion surgery study. *J Neurosurg* 119(4):988–995. <https://doi.org/10.3171/2013.6.JNS13312>
 28. Federau C, Christensen S, Zun Z, Park SW, Ni W, Moseley M, Zaharchuk G (2017) Cerebral blood flow, transit time, and apparent diffusion coefficient in moyamoya disease before and after acetazolamide. *Neuroradiology* 59(1):5–12. <https://doi.org/10.1007/s00234-016-1766-y>
 29. Derdeyn CP, Zipfel GJ, Zazulia AR, Davis PH, Prabhakaran S, Ivan CS, Aiyagari V, Sagar JR, Hantler N, Shinawi L, Lee JJ, Jafri H, Grubb RL, Miller JP, Dacey RG (2017) Baseline hemodynamic impairment and future stroke risk in adult idiopathic moyamoya phenomenon results of a prospective natural history study. *Stroke* 48(4):894–899. <https://doi.org/10.1161/strokeaha.116.014538>
 30. Setta K, Matsuda T, Sasaki M, Chiba T, Fujiwara S, Kobayashi M, Yoshida K, Kubo Y, Suzuki M, Yoshioka K, Ogasawara K (2021) Diagnostic accuracy of screening arterial spin-labeling mri using hadamard encoding for the detection of reduced cbf in adult patients with ischemic moyamoya disease. *AJNR Am J Neuroradiol*. <https://doi.org/10.3174/ajnr.A7167>

Publisher's note Springer Nature remains neutral with regard to jurisdictional claims in published maps and institutional affiliations.